

Rotating proton rich nuclei: the birth of proton bound rotational bands, high-spin giant proton halos and rotation induced extension of nuclear landscape

S. Teeti¹, A. V. Afanasjev^{1*} and A. Taninah¹

^{1*}Department of Physics and Astronomy, Mississippi State University, 75 B. S. Hood Rd, Starkville, 39762, MS, US.

*Corresponding author(s). E-mail(s): anatoli.afanasjev@gmail.com;
Contributing authors: sat386@msstate.edu; taninah.ahmad@gmail.com;

Abstract

It is shown for the first time that rotational bands which are proton unbound at zero or low spins can be transformed into proton bound ones at high spin by collective rotation of nuclear systems. This is due to strong Coriolis interaction which acts on high- N or strongly mixed M orbitals and drives the highest in energy occupied single-particle states of nucleonic configurations into negative energy domain. Proton emission from such proton bound rotational states is suppressed by the disappearance of static pairing correlations at high spins of interest. These physical mechanisms lead to a substantial extension of the nuclear landscape beyond the spin zero proton drip line. In addition, a new phenomenon of the formation of giant proton halos in rotating nuclei emerges: it is triggered by the occupation of strongly mixed M intruder orbitals. Possible experimental fingerprints of the transition from particle bound to particle unbound part of rotational bands are discussed and compared for proton and neutron rich nuclei near and beyond respective drip lines.

1 Introduction

In nuclear systems for a given proton number there is a minimum and maximum number of neutrons beyond which the formation of bound systems is impossible. These numbers define proton and neutron drip lines, respectively. In non-rotating nuclei, such drip lines are denoted here as the $I = 0$ drip lines. Proton and neutron $I = 0$ drip lines are defined (firmly or tentatively) experimentally up to $Z = 84$ and $Z = 10$, respectively [1–3]. Future experimental facilities such as FRIB and FAIR will hopefully extend experimental drip lines to higher Z (see Ref. [4] and Fig. 1 in Ref. [5]). These experimental efforts are accompanied by a

significant amount of theoretical investigations of the limits of the nuclear landscape in non-rotating nuclei [3, 6–9].

One of the interesting questions in nuclear physics is whether there are physical mechanisms which allow the extension of the nuclear landscape beyond the $I = 0$ drip lines corresponding to ellipsoidal shapes. Recent investigations allowed to identify two such mechanisms. The first one is related to an emergence of toroidal nuclear shapes in hyperheavy ($Z > 126$) nuclei which drives the proton drip line of such nuclei to substantially lower neutron numbers as compared with the one for the ellipsoidal-like shapes (see Fig. 2 in Ref.

[10] and discussion in Refs. [10–12]). In the second one, the birth of neutron bound rotational bands provides a mechanism for an extension of nuclear landscape to neutron numbers which are larger than those of the $I = 0$ neutron drip line in non-rotating nuclei [13]. The birth of such bands is due to strong Coriolis interaction acting on high- j orbitals which transforms neutron unbound (resonance) nucleonic configurations into neutron bound ones with increasing angular momentum.

Unfortunately, the experimental studies of these mechanisms with existing and near-future experimental facilities are impossible in hyper-heavy nuclei and are extremely difficult in the region of the neutron drip line. Thus, the goal of the present paper is to analyze such physical mechanisms in even Z proton-rich $4 \leq Z \leq 36$ nuclei some of which may be accessible with the next generation of experimental facilities. It will be shown that the mechanism of the birth of particle bound rotational bands is also possible in such nuclei but it is based on the occupation of proton orbitals. Another aim is to investigate the formation of giant proton halos induced by rotation in light proton rich nuclei. Finally, a systematic study of the extension of nuclear landscape due to above-mentioned mechanisms is the third objective of the paper.

Note that existing experimental studies of rotational structures in the nuclei either located beyond the proton drip line or possessing proton unbound configurations are limited in the scope and all of them are listed below. The rotational structures have been observed in proton unbound $^{175,177}\text{Au}$ and ^{144}Ho nuclei in Refs. [14, 15]. The studies of energy-spin phase space for proton rich Pt and Au nuclei near and beyond the proton drip line reveal the evidence for the limits of excitation energy and angular momentum which a nucleus beyond the proton drip line can sustain [16]. Prompt proton decays connecting five band-head states of rotational bands in ^{59}Cu with three spherical states in ^{58}Ni have been observed in Ref. [17].

The paper is organized as follows. A brief outline of the theoretical framework and the details of the calculations are presented in Sec. 2. Sec. 3 is dedicated to the analysis of the birth of proton bound rotational bands in the ^{14}Ne and ^{67}Kr nuclei. The formation of giant proton halos in rotating very proton rich nuclei is analyzed in Sec. 4. The basic

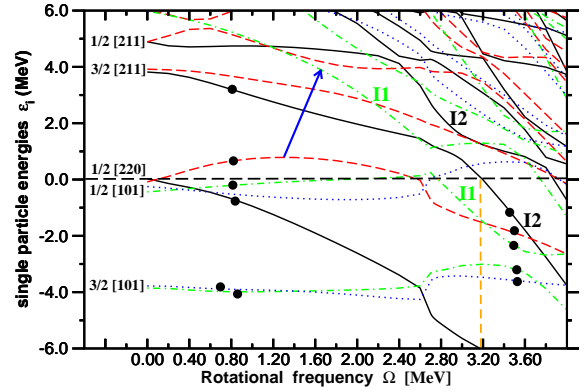


Fig. 1 Proton single-particle energies (routhians) in the self-consistent rotating potential of ^{14}Ne as a function of rotational frequency Ω . They are given along the deformation path of the $[1, 1, 1, 1] \otimes [2, 3, 3, 2]$ occupation block. Long-dashed red, solid black, dot-dashed green, and dotted blue lines indicate $(\pi = +, r = +i)$, $(\pi = +, r = -i)$, $(\pi = -, r = +i)$, and $(\pi = -, r = -i)$ orbitals, respectively. At $\Omega = 0.0$ MeV, the single-particle orbitals are labeled by the asymptotic quantum numbers $K[Nn_z\Lambda]$ (Nilsson quantum numbers) of the dominant component of the wavefunction. Solid circles indicate occupied orbitals in proton bound and proton unbound parts of the configurations. The vertical orange dashed line indicates the frequency (corresponding to spin I_{trans}) at which the configuration becomes proton bound. Intruder orbitals of the M-type before and after band crossing are labelled by I1 and I2.

physical mechanism of the birth of particle bound rotational bands in proton and neutron rich nuclei located near and beyond proton and neutron drip lines are discussed in Sec. 5. Rotation induced extension of the nuclear landscape is discussed in Sec. 6. Finally, Sec. 7 summarizes the results of our paper.

2 The details of theoretical calculations

2.1 Theoretical framework

The calculations are performed in the framework of cranked relativistic mean field (CRMF) theory [18–20]. It represents the realization of covariant density functional theory for rotating nuclei with no pairing correlations in one-dimensional cranking approximation. It has been successfully tested in a systematic way on the properties of different types of rotational bands in the regime of weak pairing such as normal-deformed, superdeformed and smooth terminating bands as well as the bands at the extremes of angular momentum (see

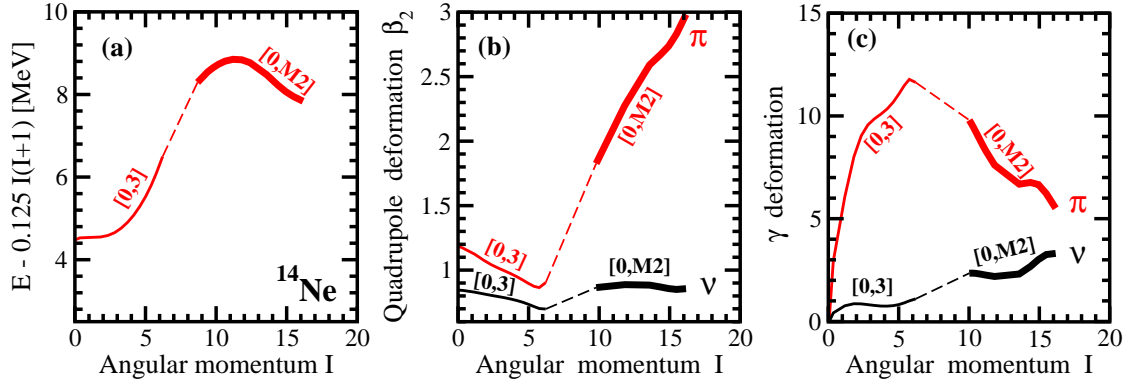


Fig. 2 The energies [relative to a smooth liquid drop reference $E_{RLD} = AI(I+1)$] and neutron and proton quadrupole (β_2) and triaxial (γ) deformations of the $[1, 1, 1, 1] \otimes [2, 3, 3, 2]$ occupation block in ^{14}Ne as a function of angular momentum I . The deformation parameters $\beta_2 = \sqrt{\frac{5}{16\pi} \frac{4\pi}{3AR_0^2} \sqrt{Q_{20}^2 + 2Q_{22}^2}}$ and $\gamma = \arctan \sqrt{2} \frac{Q_{22}}{Q_{20}}$ are extracted from respective quadrupole moments $Q_{20} = \int d^3r \rho(\vec{r}) (2z^2 - x^2 - y^2)$ and $Q_{22} = \int d^3r \rho(\vec{r}) (x^2 - y^2)$. Note that $R_0 = 1.2A^{1/3}$.

Refs. [20, 21] and references therein). We restrict ourselves to reflection symmetric shapes which are dominant deformed shapes in the nuclear chart.

Available studies of high spin properties of rotating $N \approx Z$ nuclei located in the vicinity of the part of nuclear chart under study clearly indicate that static pairing becomes negligible at high spin [21–23]. This allows safely neglect the pairing correlations in the calculations since the focus of the present study is on the parts of rotational bands which become proton bound at high spin. The spin at which the calculations without pairing become a good approximation to those with pairing depends on the mass region: it is around $I \approx 15\hbar$ in the Kr ($Z \approx 36$) region [21, 22] but decreases with lowering the proton number Z [23]. In addition, the pairing is substantially reduced due to blocking in the nucleonic configurations in which the opposite signature orbitals are not pairwise occupied [20, 24]: for such configurations the calculations without pairing reproduce experimental data even at lower spins [21, 22].

Note that the analysis of the birth of proton bound bands in proton-rich nuclei is simplified as compared with the case of the birth of neutron bound bands in neutron-rich nuclei discussed in Ref. [13] since the continuum of proton single-particle states is formed only at positive energies above the Coulomb barrier. This allows to reliably use traditional computer codes employing basis set expansion for the description of proton unbound configurations built on positive energy

proton single-particle orbitals located below the Coulomb barrier.

The CRMF calculations are carried out with the NL3* covariant energy density functional (CEDF) [25] which is the state-of-the-art functional for nonlinear meson-nucleon coupling model [3]. It is globally tested for ground state observables in even-even nuclei [3]. The CRMF and cranked relativistic Hartree-Bogoliubov (CRHB) calculations with this functional provide a very successful description of different types of rotational bands both at low and high spins [25–27].

The CRMF equations are solved in the basis of an anisotropic three-dimensional harmonic oscillator in Cartesian coordinates characterized by the deformation parameters β_0 and γ and oscillator frequency $\hbar\omega_0 = 41A^{-1/3}$ MeV (see Refs. [18, 28]). The truncation of the basis is performed in such a way that all states belonging to the major shells up to $N_F = 16$ fermionic shells for the Dirac spinors and up to $N_B = 20$ bosonic shells for the meson fields are taken into account. This truncation scheme provides very good numerical accuracy for the physical observables of interest [13].

2.2 Configuration labelling

In the calculations, the configurations are specified by the number of particles k_{par}^r (where $k = \pi$ or ν for protons and neutrons, respectively) occupying single-particle orbitals of specific parity par and signature r combinations, namely, by the occupation block $[\nu_+^+, \nu_+^-, \nu_-^+, \nu_-^-] \otimes [\pi_+^+, \pi_+^-, \pi_-^+, \pi_-^-]$.

Note that the occupied orbitals are counted from the bottom of nucleonic potential. For simplicity we use only the sign for the $r = \pm i$ signature and parity $par = \pm$ in this block. The occupation block $[\nu_+^+, \nu_+^-, \nu_-^+, \nu_-^-] \otimes [\pi_+^+, \pi_+^-, \pi_-^+, \pi_-^-]$ defines the lowest in energy configuration for a given combination of parities and signatures of occupied orbitals. This type of configuration definition is common in density functional theoretical (DFT) calculations without pairing: it is used not only in the CRMF calculations [18, 28], but also in the cranked Skyrme DFT calculations [29, 30].

The rotational and deformation properties of extremely deformed bands strongly depend on intruder content of their configurations. Thus, an alternative way of configuration labeling, frequently used in the literature, is by counting the number of occupied intruder orbitals [28, 31]. This labelling scheme is also used in the present paper since it provides important physical insight on the properties of the bands. Thus, the configurations are labeled by shorthand labels $[n, p_1 p_2]$ where n ($p_1 p_2$) indicates the number of occupied intruder neutron (proton) orbitals. However, the meaning of intruder orbitals depends on the mass region. For example, the configurations $[n, p_1]$ in ^{14}Ne are labeled by the number of occupied $N = 2$ neutron (n) and proton (p_1) intruder orbitals while those in ^{67}Kr by the number of the occupied $N = 4$ neutron (n) intruder orbitals and $N = 4$ (p_1) and $N = 5$ (p_2) proton intruder orbitals. The label p_2 is omitted when $p_2 = 0$.

Note that such labeling is feasible only in the case when more than 50% of intruder orbital wavefunction belongs to a specific N -shell. However, proton intruder orbitals, which are strongly downslowing as a function of rotational frequency in the routhian diagrams at high rotational frequencies (see Fig. 1), are significantly mixed because of the $\Delta N = 2$ interaction. For example, at rotational frequency $\Omega_x = 3.20$ MeV the squared weights a_N^2 of the $N = 2, 4, 6,$ and 8 shells in the structure of the wave function of the intruder I2 orbital of the configuration $[0, M2]$ are 0.09, 0.12, 0.19 and 0.21, respectively. Note that $\sum_N a_N^2 = 1.0$ (see Sec. D1 in Ref. [32]). As a consequence, there is no single N -shell whose contribution to the structure of the wave function exceed 50%. Such strongly mixed orbitals are called here as M-orbitals and the label "M#" is

used in the shorthand $[n, p]$ notation to indicate their presence and their number #. Note that we count total number # of negative and positive parity orbitals when we define the number of the M-orbitals.

The use of such configuration labelling and basic features of calculated configurations are illustrated in Fig. 2 on the example $[1, 1, 1, 1] \otimes [2, 3, 3, 2]$ occupation block in ^{14}Ne . Its calculated $E - E_{RLD}$ curve represents the envelope of two configurations defined in terms of the occupation of intruder orbitals, namely, the $[0, 3]$ and $[0, M2]$ [see Fig. 2(a)]. The configuration change from $[0, 3]$ to $[0, M2]$ within this occupation block is due to unpaired band crossing related to the crossing of the single-particle orbitals which takes place at rotational frequency $\Omega \approx 2.6$ MeV (see Fig. 1). It triggers substantial changes in equilibrium deformations and their evolution with angular momentum [see Figs. 2(b) and (c)].

The lines of different styles are used in Fig. 2 and throughout the paper to discriminate between different parts of the $E - E_{RLD}$ curve corresponding to a given occupation block. In this paper, proton unbound parts of the rotational bands [such as configuration $[0, 3]$ in Fig. 2] are shown by thin solid lines while the proton bound ones [such as the configuration $[0, M2]$ in Fig. 2] by thick solid line. Since the calculations are performed as a function of rotational frequency, the solutions are not available for some spin range in the region of band crossing. Thus, we use dashed thin line to connect the configurations, defined in terms of intruder orbitals, within the envelope of the specific occupation block (see Fig. 2).

2.3 Cranking model versus alternative approaches

The cranking model has a proven track of successful description of rotational structures of different types in nuclear chart (see Refs. [20, 27, 33–44]). In reality, the absolute majority of experimental rotational bands, for which theoretical description exist, have been analyzed in this framework. In particular, the CRHB and CRMF approaches have been successfully employed for the description of experimental rotational bands in paired [21, 27, 42, 45–49] and unpaired [19, 26, 28, 47, 50–54] regimes across the nuclear chart, respectively.

In the context of our studies, the cranking model offers several advantages over alternative microscopic approaches to the description of rotating nuclei. First advantage lies in the use of intrinsic (rotating) frame which allows a relatively simple and reliable definition of the transition point from particle unbound to particle bound part of rotational band (see discussion in Secs. 5.1 and 5.2).

Second advantage is related to the use of the large basis space which allows to take into account the mixing of different N shells in the structure of the single-particle states and the drastic changes in the equilibrium deformations of the configurations with increasing spin (see discussion in Secs. 2.2 and 4).

The third advantage lies in the separation of the model space into particle-hole and particle-particle channels. The latter includes the pairing correlations which as discussed above are negligible at high spins of interest and thus can be neglected. In such a situation the physical problem is reduced to the particle-hole channel which takes into account all available correlations including those related to the deformation and rotational responses of the nucleus. Note that the single-particle states in rotating frame include all these correlations and, in particular, those related to the response to the Coriolis force which makes intruder orbitals strongly downslowing with increasing rotational frequency (see Fig. 1 and Sec. 5.1). As a consequence, at high spin the problem is reduced to an extreme example of independent particle model in the rotating frame [52, 55–57]: the rotating nucleonic potential includes all available correlations and the energy of the last occupied single-particle state with respect of the zero energy threshold in proton rich nuclei or continuum threshold in neutron rich ones provides the information of whether the nucleus is bound or unbound with respect of particle decay at given spin (see Sec. 5 for more details).

The properties of low spin rotational bands in light and medium mass nuclei are studied also in spherical shell motivated models including *ab initio* ones (see, for example, Refs. [58–60]). However, the rotational bands of interest which become proton bound at high spin are extremely deformed in the proton subsystem (see Sec. 4 below) and are built on intruder proton M-orbitals the wave functions of which include components

from extremely high N shells (see example in Sec. 2.2 and Sec. 3 below). This requires enormous increase of configuration space and, as a consequence, such models cannot handle extremely deformed configurations because of numerical reasons. The $A \approx 60$, $N \approx Z$ region is one of such examples. Highly- and superdeformed bands in this region are successfully described within the cranked versions of relativistic and non-relativistic density functional theories [51, 61] but they are outside the applicability range of spherical shell motivated models (see Ref. [62]).

Rotational structures are frequently described also in projected shell model (see, for example, Refs. [63, 64]) which provides good description of experimental data in many regions. However, this model requires as an input the parameters related to the equilibrium deformation of the system. In addition, the calculation are performed in a limited configuration space spanning three major shells. As a consequence, it is not self-consistent in nature and is not able to describe the drastic changes in the deformation with increasing spin which take place in the nuclei of interest.

Note that it is very difficult to establish the transition point from particle bound to particle unbound part of rotational band in the models formulated in the laboratory frame. To do that the studies of all possible decay channels from a given state with spin I and their evolution with spin are required. However, as mentioned above this is impossible because of numerical reasons for extremely deformed configurations of interest.

3 The birth of proton-bound rotational bands in ^{14}Ne and ^{67}Kr nuclei

To illustrate the basic features of rotation in very proton rich nuclei and their dependence on the mass region we consider the examples of the ^{14}Ne and ^{67}Kr nuclei. ^{14}Ne is an extremely proton rich nucleus with 10 protons and only 4 neutrons and ^{67}Kr has 36 protons and 31 neutrons. In the Ne isotopic chain the last proton bound even-even nucleus is ^{18}Ne in the RHB calculations at spin $I = 0$ which agrees with the fact that experimentally measured ^{16}Ne is located beyond the two-proton drip line [3]. These calculations also predict that the last proton bound Kr isotope is

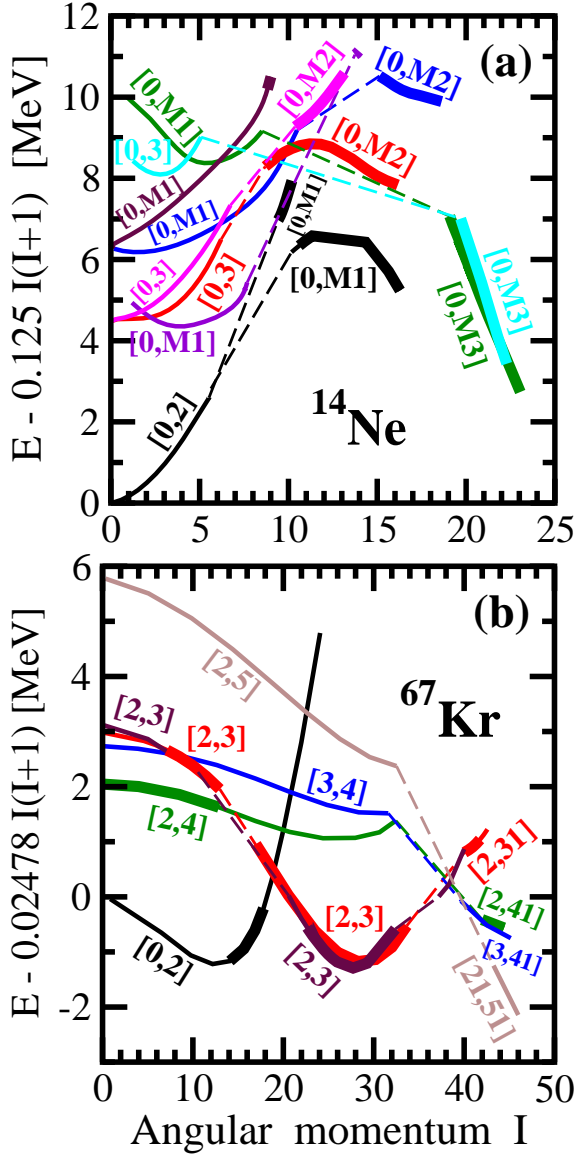


Fig. 3 The energies of calculated configurations in ^{14}Ne and ^{67}Kr relative to a smooth liquid drop reference $AI(I+1)$. The numerical values of inertia parameter A are indicated on vertical axis. Additional information on the configurations of these nuclei are displayed in Table 1.

^{68}Kr . This is in agreement with the observation of two proton radioactivity in ^{67}Kr [65, 66].

The calculated configurations of the ^{14}Ne and ^{67}Kr nuclei are shown in Fig. 3. One can see that absolute majority of the configurations in these nuclei are proton unbound at low spin but with increasing spin and undergoing band crossing these configurations become proton bound. The microscopic origin of this transition is illustrated

Table 1 The configurations calculated in the ^{14}Ne and ^{67}Kr nuclei. The first column specifies the occupation blocks of the configurations. The second column identifies the configurations in terms of intruder orbitals corresponding to the respective occupation block: the first/second label corresponds to low/high spin configurations. The total parity π_{tot} and signature r_{tot} of the occupation block are listed as (π_{tot}, r_{tot}) in the last column.

| occupation block | configurations | (π_{tot}, r_{tot}) |
|---------------------------------------|------------------|------------------------|
| 1 | 2 | 3 |
| ^{14}Ne [$N = 4, Z = 10$] | | |
| $[1, 1, 1, 1] \otimes [2, 2, 3, 3]$ | $[0,2], [0,M1]$ | $(+, +)$ |
| $[1, 1, 1, 1] \otimes [2, 3, 3, 2]$ | $[0,3], [0,M2]$ | $(-, +)$ |
| $[1, 1, 1, 1] \otimes [1, 3, 4, 2]$ | $[0,M1], [0,M3]$ | $(+, +)$ |
| $[1, 1, 1, 1] \otimes [2, 2, 4, 2]$ | $[0,M1], [0,M2]$ | $(+, -)$ |
| $[1, 1, 1, 1] \otimes [2, 2, 2, 4]$ | $[0,M1], [0,M1]$ | $(+, -)$ |
| $[1, 1, 1, 1] \otimes [1, 2, 4, 3]$ | $[0,M1], [0,M2]$ | $(-, +)$ |
| $[1, 1, 1, 1] \otimes [1, 4, 3, 2]$ | $[0,3], [0,M3]$ | $(-, -)$ |
| $[1, 1, 1, 1] \otimes [3, 2, 3, 2]$ | $[0,3], [0,M2]$ | $(-, -)$ |
| $[1, 1, 1, 1] \otimes [2, 2, 3, 3]$ | $[0,2], [0,M1]$ | $(+, +)$ |
| ^{67}Kr [$N = 31, Z = 36$] | | |
| $[7, 7, 9, 8] \otimes [8, 8, 10, 10]$ | $[0,2]$ | $(-, +)$ |
| $[8, 8, 8, 7] \otimes [8, 9, 9, 10]$ | $[2,3], [2,3]1$ | $(+, -)$ |
| $[8, 8, 8, 7] \otimes [9, 9, 9, 9]$ | $[2,4], [2,4]1$ | $(-, +)$ |
| $[8, 9, 7, 7] \otimes [9, 9, 9, 9]$ | $[3,4], [3,4]1$ | $(+, -)$ |
| $[8, 8, 7, 8] \otimes [8, 9, 10, 9]$ | $[2,3], [2,3]1$ | $(+, -)$ |
| $[8, 8, 8, 7] \otimes [10, 9, 9, 8]$ | $[2,5], [2,5]1$ | $(+, -)$ |

in Fig. 1 on the example of proton single-particle routhian diagram corresponding to the $[1, 1, 1, 1] \otimes [2, 3, 3, 2]$ occupation block which leads to the $[0, 3]$ and $[0, M2]$ configurations (in terms of intruder orbitals) at low and high spins [see red lines in Fig. 3(a)], respectively. At low and medium rotational frequencies Ω_x , the occupied proton $1/2[220](r = +i)$ and $3/2[211](r = -i)$ orbitals are located at positive energies [see Fig. 1(a)]. Thus, the $[0, 3]$ configuration is proton unbound. However, with increasing rotational frequency intruder orbitals $I1$ and $I2$ of negative and positive parities become occupied at $\Omega_x \approx 2.9$ MeV leading to the $[0, M2]$ configuration which becomes proton bound at $\Omega = 3.19$ MeV. This microscopic mechanism of the creation of proton bound rotational bands from proton unbound ones is equivalent to the birth of particle bound rotational bands in very neutron rich nuclei near neutron drip line discussed earlier in Ref. [13].

An interesting feature of these rotational structures is the fact that at least 80% of the angular momentum is built in the proton subsystem because of limited angular momentum content

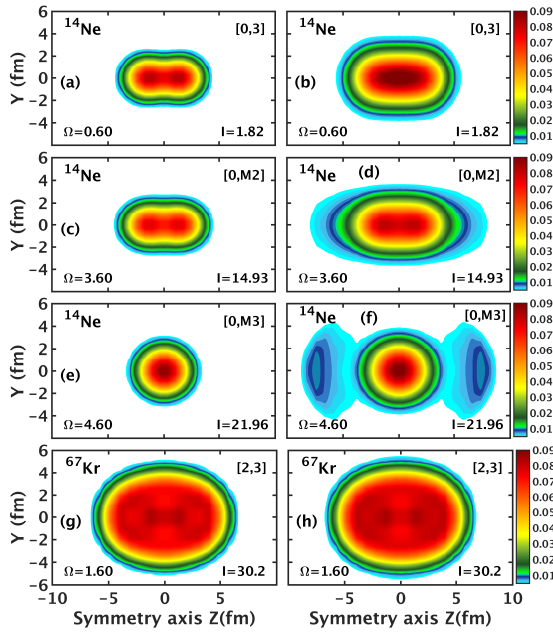


Fig. 4 Neutron (left column) and proton (right column) density distributions of the configurations in ^{14}Ne and ^{67}Kr at indicated spins and frequencies. The density colormap starts at $\rho = 0.005 \text{ fm}^{-3}$ and shows the densities in fm^{-3} .

in the neutron one. Thus, the neutron subsystem behaves as a spectator in building collective rotation.

By performing the calculations for the ^{14}Ne nucleus with the DD-MEX [67] and NL1 [68] covariant energy density functionals it was verified that the general results obtained in the present paper are not affected by the selection of the functional. This can be understood in the following way. The general single-particle structure, the energies of the single-particle states with respect of zero energy threshold and their response to deformation obtained in the calculations with NL3*, NL1 and DD-MEX are similar at no rotation. Some differences between the CEDFs in the energies of the single-particle states are not critical because of their low level densities near the Fermi level. The response of the nuclei to the rotation depends on the alignments of the single-particle orbitals which are visualized by the slopes of the single-particle energies as a function of rotational frequency in Fig. 1. For a given single-particle orbital and for the same deformation, the alignment almost does not depend on the functional. The low-spin configurations have a limited angular momentum content (see Refs. [23, 36, 40]). Thus,

high angular momentum configurations are built within the occupation block by occupying high- N or mixed M intruder orbitals which have substantial angular momentum content. For example, this corresponds to the transition from the $[0,3]$ to $[0, M2]$ configurations in the $[1, 1, 1, 1] \otimes [2, 3, 3, 2]$ occupation block. The similarity of the single-particle structure between functionals persists also after band crossing: it leads to the similarity of the calculated densities and deformations. As a consequence, obtained results depend more on the underlying single-particle structure and its response to deformation and rotation than on the isovector properties of the functional or how the density dependence [explicitly (as in DD-MEX) or implicitly (as in NL3*)] is treated. This is well illustrated by the results obtained with NL1, which is the first successful CEDF generated 36 years ago [68]. Its isovector properties are worse as compared with the ones of the NL3* and DD-MEX functionals. However, this functional produces a reasonable single-particle spectra (see Ref. [69]) and this is a reason why the results obtained with this functional are close to those shown in Fig. 3(a) obtained with NL3*. However, some dissimilarities of the single-particle energies of the occupied states seen between employed functionals will somewhat affect the relative energies of calculated configurations, and within the occupation block the frequency of unpaired band crossing and the frequency at which the band becomes proton bound. However, in no way these differences between the functionals will affect the fact that rotational bands of interest become proton bound at high spin.

4 Giant proton halo in rotating very proton-rich nuclei

The above discussed features and transition to exceedingly proton rich nuclei lead to significant modifications in density distributions which are especially pronounced in light nuclei. For example, the imbalance between protons and neutrons leads to a substantial proton skin and/or halo already at low spin in all calculated configurations of ^{14}Ne . This is illustrated by the comparison of neutron and proton densities of the $[0, 3]$ configuration in Figs. 4(a) and (b). Additional proton particle-hole

excitations leading to the $[0, M2]$ configuration generate low density giant proton halo which is especially extended in the equatorial region [see Fig. 4(d)]. Note that this particle-hole excitation has only small impact on the neutron densities (compare Figs. 4(a) and (c)) indicating that there is a substantial decoupling of proton and neutron degrees of freedom due to underlying shell structure.

These two subsystems of the $[0, M2]$ configuration have drastically different quadrupole (β_2) and triaxial (γ) deformations which also behave differently as a function of angular momentum [see Fig. 2(b) and (c)]. The β_2 and γ deformations of the neutron subsystem almost do not change with increasing angular momentum. In contrast, the quadrupole deformation β_2 of proton subsystem drastically increases with increasing angular momentum due to the centrifugal stretching of the nucleus [see Fig. 2(b)]. Similar (but significantly less pronounced) processes have been seen before in the calculations of many hyper- and megadeformed rotational bands in the $A \approx 40$ $N \approx Z$ (see Ref. [23]) and $Z = 40 - 58$ (see Ref. [32]) regions of nuclear chart. The γ -deformation of proton subsystem decreases fast with increasing angular momentum.

Additional particle-hole excitations lead to more exotic nuclear shapes. For example, the excitation indicated by blue arrow in Fig. 1 leads to the occupation block $[1, 1, 1, 1] \otimes [1, 3, 4, 2]$ which corresponds to the envelope of the $[0, 3]$ and $[0, M3]$ configurations shown in cyan in Fig. 3. The densities of low spin $[0, 3]$ configuration are similar to those shown in Fig. 4(a) and (b). However, the ones for the high spin $[0, M3]$ configuration are built of near spherical shape for neutron densities [Fig. 4(e)] and cluster-type giant proton halo in proton subsystem [Fig. 4(f)]. The latter consist of high density prolate central cluster and low (with $\rho \approx 0.01 \text{ fm}^{-3}$) density clusters centered at around $z \approx \pm 7 \text{ fm}$.

The kinematic moments of inertia $J^{(1)}$ and transition quadrupole moments Q_t of the bands with giant proton halos are substantially larger than those of the ground state rotational band. For example, in the ^{14}Ne nucleus the kinematic moment of inertia of the ground state band is $J^{(1)} \approx 2.2 \text{ MeV}^{-1}$ at spin $I = 2\hbar$, while that for the $[0, M3]$ configurations shown in Fig. 1(a)

is $J^{(1)} \approx 5.3 \text{ MeV}^{-1}$ at $I \approx 20\hbar$. The Q_t values for the ground state and giant proton halo rotational bands are $Q_t \approx 0.55 \text{ eb}$ and $Q_t \approx 1.4 \text{ eb}$, respectively. These large differences in the physical observables could be used for an experimental identification of potential candidates for giant proton halo structures.

Note that the processes of the creation of proton halos are suppressed in higher Z nuclei due to smaller imbalances between protons and neutrons and reduced relative impact of a given single-particle orbital into the buildup of the total densities. This is illustrated by the comparison of the proton and neutron density distributions in the $[2, 3]$ configuration of ^{67}Kr [Figs. 4(g) and (h)].

The physical mechanism of the creation of giant proton halos in rotating nuclei is completely different as compared with that predicted for non-rotating proton rich nuclei. In the latter ones, it is based on the occupation of loosely bound s and p orbitals [70–72]. In contrast, it is due to either a significant excess of protons over neutrons [compare Figs. 4(a) and (b)] or the occupation of intruder strongly-mixed M-orbitals [Figs. 4(d) and (f)]. The wave functions of the later ones contain significant admixtures from the high N shells (see example in Sec. 2.2). Note also that in many cases these orbitals are deeply bound: the Fermi levels, corresponding to the energy of the last occupied orbital, of the configurations of interest is located in the range between -4 to -2.5 MeV at the highest calculated rotational frequencies (see, for example, Fig. 1). The nodal structure of these intruder orbitals (see discussion in Ref. [73]) plays an important role in the creation of the halo and cluster type structures of rotating nuclei under study.

5 Basic physical mechanisms of the birth of particle bound rotational bands

It is important to outline the basic physical mechanisms leading to the birth of particle bound rotational bands and observable features of this transition which could be potentially measured in future experiments. These results are born in the analysis of the results of the calculations carried out in the present paper and in Ref. [13].

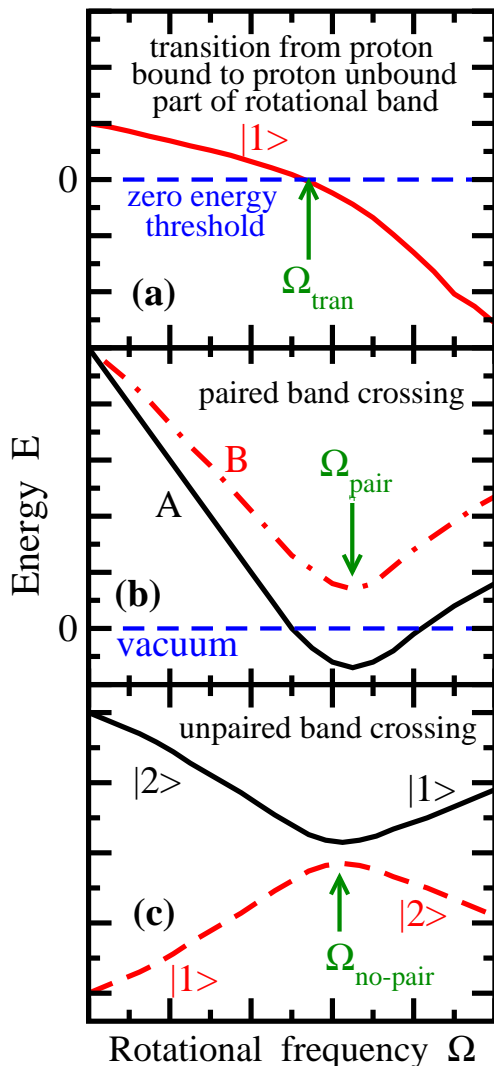


Fig. 5 Schematic comparison of the transition from proton unbound to proton bound part of rotational band in near proton-drip line nuclei [panel (a)] with paired [panel (b)] and unpaired [panel (c)] band crossings in rotating nuclei (see text for detail).

5.1 The occupation of strongly downsloping intruder orbitals

The birth of particle bound rotational bands in the nuclei near and beyond spin zero proton and neutron drip lines is connected with the occupation of either high- N or mixed M intruder orbitals which are strongly downsloping with increasing rotational frequency. The underlying physics is illustrated in Fig. 5(a). At low rotational frequency, the highest in energy occupied orbital of the nucleonic configuration of interest, shown by

red line in Fig. 5(a), is located at positive energies. In neutron rich nuclei, this leads to neutron emission and formation of resonance parts of rotational bands (see Ref. [13]). The proton emission is expected to take place at low and medium rotational frequencies in proton-rich nuclei (see Sec. 5.2). Note that strong Coriolis force acts upon such orbitals because of their high- N or M content. As a consequence, these orbitals, located at positive energies at low frequency, dive into the region of negative energies with increasing rotational frequency. In proton rich nuclei, they become proton bound at rotational frequency $\Omega > \Omega_{tran}$ when the highest in energy occupied proton single-particle state crosses zero energy threshold at frequency Ω_{tran} (see Fig. 5(a) and Secs. 5.2 and 3). The same mechanism is also active in neutron rich nuclei (see Ref. [13]).

When discussing such a transition it is important to understand (i) whether the cranking description in rotating frame provides a proper reproduction of energy evolution of the intruder orbitals with spin or rotational frequency and their crossing with continuum threshold in neutron rich nuclei or zero energy threshold in proton rich nuclei and (ii) how well the particular model, namely, the CRMF approach performs in that respect. The transition from proton unbound to proton bound part of rotational band is defined by the relative evolution in energy of the last occupied single-particle state of nucleonic configuration and zero-energy threshold (see Fig. 5a). In this respect, it is extremely similar to the description of paired and unpaired band crossings in rotating nuclei.

In cranking model description of rotating nuclei with pairing included, two-quasiparticle configuration $A+B$ ¹ which is located at some excitation energy with respect of quasiparticle vacuum at zero frequency gets lower in energy with increasing rotational frequency and becomes a vacuum configuration at some frequency Ω_{pair} (see Fig. 5b). This change in vacuum configuration leads to a paired band crossing (see Refs. [33–35, 74]). The experimental data related to the evolution of the energies of quasiparticle states with frequency and the properties of paired band crossings (the frequency of crossing and the gain in

¹The conventional labelling of quasiparticle orbitals by letters A, B, ... (see Ref. [74]) is used here.

alignment at the crossing) in rotational bands are, in general, well described in cranked shell model based on phenomenological potentials [33, 44, 74] and non-relativistic DFTs based on Gogny and Skyrme forces [37, 38, 75]. Extensive and systematic studies of normal deformed bands in the $A \sim 70, N \approx Z$ [21], rare-earth [76] and actinide [27, 47] regions of the nuclear chart as well as of superdeformed bands in the $A \sim 190$ mass region [42] reveal that very good description of rotational properties and band crossing features is obtained in the CRHB framework.

Unpaired band crossings emerge from the crossing of two single-particle orbitals with the same quantum numbers which are separated by some energy at zero frequency/spin. This is illustrated in Fig. 5(c) where the lowest (highest) in energy single-particle orbital is occupied (empty) at all frequencies. At low frequencies, the lowest and highest in energy orbitals of this pair are labelled by $|1\rangle$ and $|2\rangle$. However, they exchange their character at crossing frequency $\Omega_{no-pair}$ (see Sec. 2.3.5 in Ref. [35] and Sec. 12.4 in Ref. [36] for more detailed discussion of unpaired band crossings). The crossing frequency $\Omega_{no-pair}$ depends both on the relative energies of these orbitals at low frequency and on their alignment properties. The cranking models with single-particle orbitals, defined in rotating frame, reasonably well describe their alignment properties (which define the change of single-particle energies with frequency/spin) extracted from experimental data. This was systematically verified both in the cranked Nilsson-Strytinsky (CNS) [21, 40, 51, 55] and the CRMF [21, 51, 52] approaches. It is interesting that on average these properties are better described in the CRMF approach [21, 51, 77]. The relative energies of the single-particle states in such pairs of crossing orbitals are also reasonably well described with better description provided by the CNS approach. As a consequence, the rotational and band crossing features of experimentally known rotational bands undergoing unpaired band crossing are reasonably well described in model calculations (see, for example, Refs. [28, 40, 53]).

These results clearly indicate that the cranking description in rotating frame well reproduces the change of the energies of the single-particle states with rotational frequency. Good agreement with experiment obtained in the cranking model

calculations of rotational and band crossing properties proves that such a description is a good approximation to the description in the laboratory frame. Indeed, the equivalence of the description of rotating nuclei in the intrinsic (rotating) and laboratory frames was confirmed with good accuracy in Ref. [78] on the example of ^{48}Cr .

This analysis also suggests that that the transition from particle unbound to particle bound part of rotational band takes place at approximately the same spin (or frequency) in rotating and laboratory frames. Model description of this transition is simpler than the description of band crossings because the single-particle orbital does not interact with zero-energy threshold. On the contrary, there is an interaction of the single-particle states at and near band crossing resulting in the repulsion of the single-particle orbitals [see Fig. 5(b) and (c)].

It is also important to keep in mind that the zero energy threshold as a point of transition from negative to positive energies for the single-particle states should not be treated as something static given at spin zero once and forever: it depends on the configuration and respective collective coordinates (deformations and rotational frequency).

5.2 The mechanism of suppression of proton emission at high spin

To our knowledge, no proton emission from the states which rotate collectively has been observed so far in experiment. In all known cases of proton emission from the states of rotational bands, such emission is observed from the state(s) which represent the band-head(s) of rotational band(s). The band-head is either the ground state (as in the case of ^{141}Ho [15]) or isomeric state (as in the case of ^{141}Ho [15]) or particle-hole excited states (as in the case of ^{59}Cu [17]) on top of which collectively rotating states are built. This non-observation of proton emission from rotating states is due to typical γ -decay time $\tau_\gamma \approx 10^{-9}$ s of the states in rotational band being much shorter than typical experimentally observable half-lives τ_π (from 10^{-6} s to a few seconds) of proton emission in medium mass nuclei [79]. It is only recently that $\tau_\pi \approx 4.5 \cdot 10^{-7}$ s become achievable in experiment [80]. As a consequence, at present the rotational

states of rotational band are connected only by the γ -transitions in experiment.

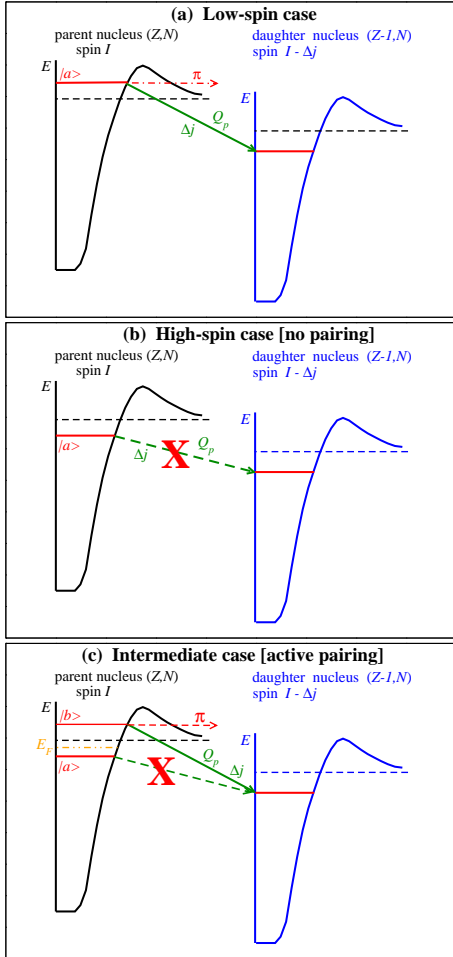


Fig. 6 Schematic illustration of proton emission process in different cases discussed in the text. For both parent and daughter nuclei the states of interest are indicated by red lines in respective proton potentials. Horizontal dashed lines indicate zero energy thresholds. Possible proton emission through Coulomb barrier is indicated by red dot-dashed arrows. Green solid lines indicate the transition between nucleonic configurations in parent and daughter nuclei: the Q_p and Δj values associated with this transition are displayed. These lines become dashed for the transitions which are permitted from energy point of view ($Q_p > 0$) but forbidden because the state of interest $|a\rangle$ is proton bound in the parent nucleus. In panel (c), orange dot-dashed line shows the position of the proton Fermi level E_F .

The observation of the competition of γ -decay and proton emission from a given rotational state requires that significantly shorter half-lives τ_π can be measured in experiment. Assuming that this

will be possible in future experiments, it is important to at least conceptually understand how the proton emission will evolve with spin within the rotational band which undergoes the birth of proton bound rotational states. Fig. 6 is used to illustrate the main aspects of this process. Note that in general several proton emission channels are possible from a given rotational state. However, for simplicity of discussion we consider only one in Fig. 6. The main features of above mentioned processes are the following:

1. **The proton emission from the band-heads of rotational bands** is illustrated in Fig. 6(a). The last proton in the parent nucleus occupies the single-particle state $|a\rangle$ with positive energy and has the final probability to penetrate the Coulomb barrier. The structure of this state defines how much angular momentum Δj can be carried away by emitted proton. Proton emission half-lives τ_π are defined by the Q_p energies, angular momentum carried away by proton and the wavefunctions of initial and final states [81]. The Q_p energies depend on the difference in the binding energies of the states in parent and daughter nuclei [79, 80, 82]. Note that the presence of pairing would reduce the occupation probability of the $|a\rangle$ state and modify its τ_π values but would not affect the fact of proton emission.
2. **Proton emission from low or medium spin I rotational state in parent nucleus to the rotational state with spin $I - \Delta j$ in daughter nucleus.** At such spins, static pairing correlations still play a role and the physics discussed in point (1) and illustrated in Fig. 6(a) remains valid but with some modifications discussed below.

Existing formalisms for the description of proton emission from rotating states are based on some variations of particle+rotor model [81] which assumes the same deformations for parent and daughter nuclei. However, we are not aware of any publication in which the evolution of the proton emission decay properties (such as half-lives τ_π and related widths Γ) has been studied as a function of the spin I of the parent nucleus. It is only in Ref. [83] (Refs. [84, 85]) in which proton emission from ^{145}Tb (^{141}Ho) to rotational 2^+ state of the ground state band in ^{144}Er (^{140}Dy) has been theoretically analyzed.

Thus, it would be interesting to evaluate a potential impact of rotation on proton emission. Assuming rigid rotation [rotational energy given by $E_I = \frac{\hbar^2}{2J}I(I+1)$] and the same moment of inertia J in the parent and daughter nuclei the rotational contribution to the Q_p energy will be given by

$$\begin{aligned}\Delta E_{rot} &= E_I(\text{parent}) - E_{I-\Delta j}(\text{daughter}) \\ &= \frac{\hbar^2}{2J}\Delta j(2I - \Delta j - 1).\end{aligned}\quad (1)$$

Under these assumptions, the rotational contribution to Q_p will linearly increase with spin of the rotational state in the parent nucleus making τ_π shorter.

While these assumptions may be reasonable in some medium to heavy mass nuclei characterized by rigid deformation, that is not a case in the light nuclei of interest. This is because the equilibrium deformations (not only in quadrupole but also in triaxial directions) between the rotational states of interest in parent and daughter nuclei can differ drastically. This alone invalidates the applicability of particle+rotor like models (PRM) to the description of proton emission in light rotating nuclei. But there are other factors. The rotation of nuclei leads to Coriolis anti-pairing effect which is especially pronounced (as a function of spin) in light nuclei; this effect cannot be taken into account in the PRM models. In addition, this type of models is applicable only up to the first band crossing and even in this short spin range it relies on variable moment of inertia (VMI) approximation in description of rotational properties (see, for example, Refs. [84, 85]). But this approximation is not justified in light nuclei since equilibrium deformations change rapidly with angular momentum [see Figs. 2(b) and (c)]. On the other hand, these factors are taken into account in the cranking models which can reasonably well describe the evolution of binding energies and equilibrium deformations with angular momentum. However, they are not applicable for the description of proton emission.

Thus, at present there are no reliable theoretical tools which could describe the details of proton emission from rotating states in light nuclei. The situation here is reminiscent to the

one with proton emission in ^{59}Cu : it proceeds from deformed states in the parent nucleus to spherical states in daughter nucleus [17]. Because of this large change in deformation it is impossible to describe the details of proton emission with existing theoretical tools.

3. **Suppression of proton emission from high-spin states in unpaired regime.** The situation changes drastically and becomes significantly simplified for the high spin proton bound parts of rotational bands in the case of no pairing. This is illustrated in Fig. 6(b). The highest in energy occupied single-particle state $|a\rangle$ of such bands in parent nucleus is located at negative energy in rotating proton potential (frequently several MeV below zero energy threshold) [see Sec. 3 and 5.1]. Even if energetically the proton emission is permitted ($Q_p > 0$), it will not take place because the proton is bound in this state since at negative energies it faces infinite nuclear potential in spatial directions.
4. **Intermediate situation.** It is interesting to consider an intermediate situation in which the state of interest $|a\rangle$ (the situation discussed in previous point) is still located at negative energies but the pairing is present. The pairing will lead to a scattering of protons from the states located below the Fermi level to the states located above it. In particular, it can lead to an occupation of the single-particle states located above zero energy threshold [for example, the state $|b\rangle$ in the parent nucleus, see Fig. 6(c)]. In such a case, the proton emission from the state $|a\rangle$ will still be prohibited (see discussion in previous point), but the proton emission from the state $|b\rangle$ will be permitted because of its partial occupation due to pairing. The analysis of the calculations indicate that such situation can take place at low and intermediate spins.

The present analysis clearly indicates that the situation with proton emission from high spin rotational states of the bands which undergo the birth of proton bound parts is drastically different as compared with the one at low and intermediate spins. At such spins, fast rotation and multiply particle-hole excitations destroy static pairing correlations. As a consequence, the energy of the highest occupied single-particle state of nucleonic

configuration with respect of zero energy threshold in rotating proton potential defines whether the proton is bound or unbound.

5.3 Experimentally observable consequences

An interesting question is what are the experimentally observable consequences of the transition from particle bound to particle unbound parts of rotational bands with decreasing spin. The rotational states in the band are connected by the γ -transitions with typical γ -decay half-life $\tau_\gamma \approx 10^{-9}$ s. Note that the observation of the γ -transition from a rotational state with spin I' depend on the relation between $\tau_\gamma(I')$ and the timescales of alternative decay channels such as half-lives $\tau_\nu(I')$ of neutron emission in very neutron-rich nuclei (see Ref. [13]) or half-lives $\tau_\pi(I')$ of proton emission in very proton-rich nuclei.

Let us start the analysis from the rotational bands which undergo the birth of neutron bound parts at high spin in neutron rich nuclei (see Ref. [13]). At high spins the rotational states of such bands are neutron bound since the highest in energy occupied neutron single-particle state of their configurations is located at negative energy in rotating neutron potential [see single-particle states labeled with spins I , $I-2$, $I-4$ and $I-6$ of their rotational states in Fig. 7(a)]. As a result, the discrete γ -transitions are expected between such rotational states [see Fig. 7(c)]. The highest in energy occupied neutron single-particle state of the configurations of rotational states with spin $I-8$ and $I-10$ is located at positive energy [see Fig. 7(a)] and its energy increases with decreasing spin. As a consequence, because of coupling with neutron continuum these rotational states acquire some width which increases with decreasing spin [see Fig. 7(c)]. Neutron emission becomes possible from these states and dependent on the relation of the γ -decay and neutron emission half-lives three scenarios are possible, namely,

- If $\tau_\nu(I') \ll \tau_\gamma(I')$, only neutron emission will be observed from the $I' = I-8$ and $I' = I-10$ rotational states. In addition, the γ -transitions from the $I-6$ state to the $I-8$ state will acquire some width because of the width of the $I-8$ rotational state.

- If $\tau_\nu(I') \approx \tau_\gamma(I')$, both neutron emissions and γ -decays can be observed from the $I' = I-8$ and $I' = I-10$ rotational states. Note that the γ -transitions from the $I-6$ to $I-8$ state and from the $I-8$ to $I-10$ state will have some width which will be larger for the latter transition. This is because the width of rotational state is expected to increase with decreasing spin (see discussion in Ref. [13]).
- If $\tau_\nu(I') \gg \tau_\gamma(I')$, only γ -decays can be observed from the $I' = I-8$ and $I' = I-10$ rotational states. However, similar to previous point the $(I-6) \rightarrow (I-8)$ and $(I-8) \rightarrow (I-10)$ γ -transitions will not be discrete since they will possess some width.

Such γ -transitions and neutron emissions can be measured with existing experimental devices which also provide coincidence information. The point of transition from neutron bound to neutron unbound part of rotational band with decreasing spin is clearly manifest by broadening of the $(I-6) \rightarrow (I-8)$ transition [see Fig. 7(c)], the measurement of which is possible by means of γ -spectroscopy in all three cases discussed above.

While the unique and reliable experimental identification of the transition from neutron bound to neutron unbound part of rotational band is possible in neutron rich nuclei at present, the situation is much more complex on the proton-rich side of nuclear landscape. This is because the shortest observed proton emission half-life $\tau_\pi \approx 4.5 \cdot 10^{-7}$ s [80] is significantly larger than typical γ -decay half-life $\tau_\gamma \approx 10^{-9}$ s. As a consequence, the rotational states of both proton bound and proton unbound parts of rotational band will be connected by discrete² γ -transitions in the configurations of interest in the experiments with existing experimental facilities. As a result, there will be no way to experimentally identify the transition point between proton bound and proton unbound parts of rotational band for presently measured lowest τ_π values.

Assuming that τ_π can be reduced by several orders of magnitude to sub- 10^{-9} s time range in future experimental facilities, the following experimental observations will become possible:

²Note that the rotational states, built on proton configurations the highest in energy occupied single-particle state of which is located at positive energy but below the Coulomb barrier, will be discrete.

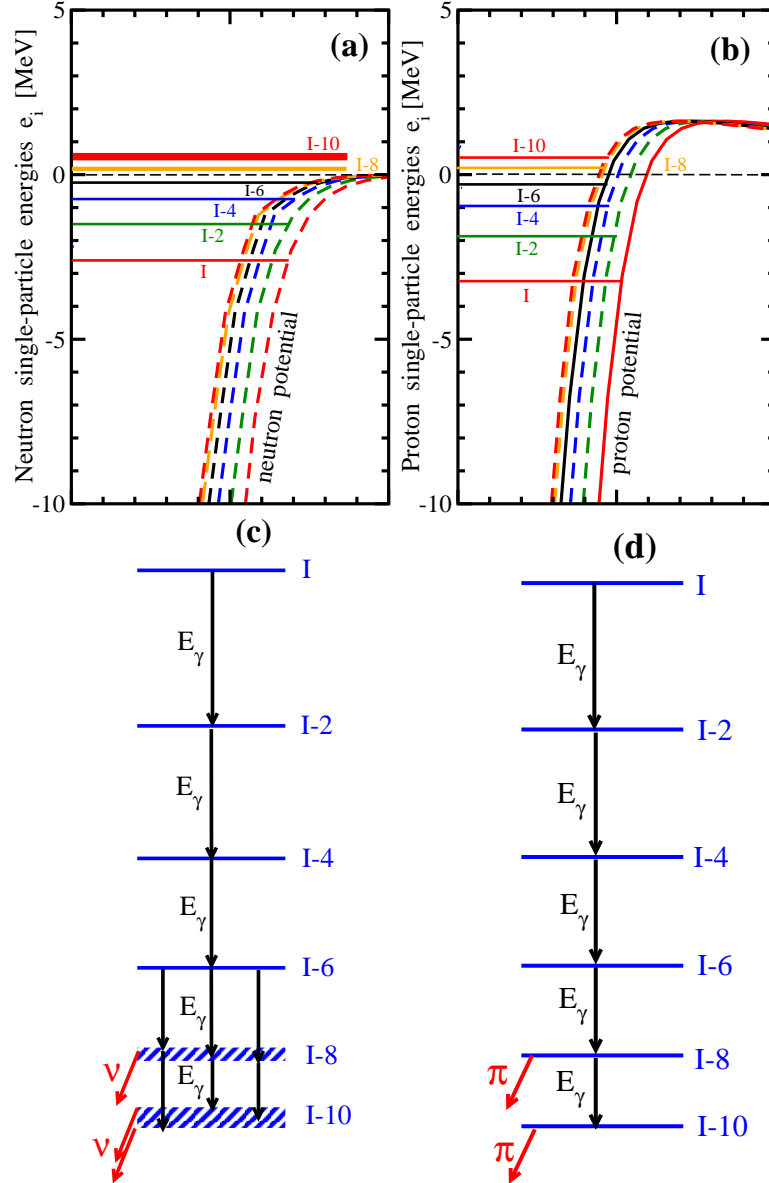


Fig. 7 Schematic illustration of the properties of rotational bands which undergo the birth of particle bound parts and their decay channels in very neutron-rich [panels (a) and (c)] and very proton-rich [panels (b) and (d)] nuclei, see text for details. Panels (a) and (b) show the energies [given by straight horizontal lines] of the highest occupied single-particle states in rotating neutron (panel (a)) and proton (panel (b)) potentials for the rotational states with spin I' for six values of I' . The dependence of respective potentials on spin is also schematically illustrated; it is due to large deformation changes with angular momentum (see Fig. 2 and Sec. 4 in the present paper and the discussion of Fig. 5 in Ref. [13]). Note that at a given spin the same color is used for potential and single-particle state in panels (a) and (b).

- **The $\tau_\pi(I') \ll \tau_\gamma(I')$ case.** The proton emission from the $I' = I - 8$ and $I' = I - 10$ states could possibly be observed [see Fig. 7(d)]. The $(I - 6) \rightarrow (I - 8)$ transition of Fig. 7(d) will be discrete since the highest in energy occupied

proton single-particle state corresponding to the $(I - 8)$ rotational state is still located below the Coulomb barrier [see Fig. 7(b)].

- **The $\tau_\pi(I') \approx \tau_\gamma(I')$ case.** Competing proton emissions and γ -decays from the $I' = I - 8$ and

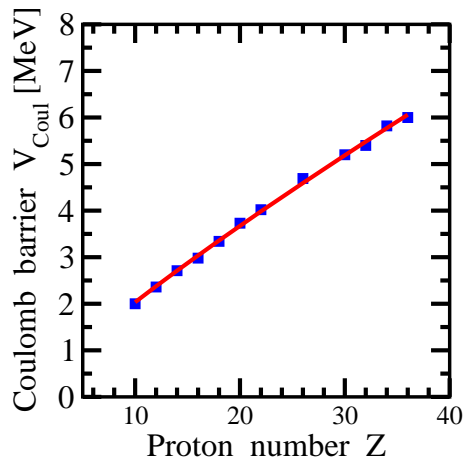


Fig. 8 The height V_{Coul} of the Coulomb barrier at spherical shape in the $N = Z$ nuclei as a function of proton number Z . Blue circles show the nuclei for which the calculations have been carried out. Red line shows the average trend of the evolution of V_{Coul} with proton number.

$I' = I - 10$ states are expected to be observed [see Fig. 7(b)].

- **The $\tau_\pi(I') \gg \tau_\gamma(I')$ case.** Only γ -transitions from the $I' = I - 8$ and $I' = I - 10$ states are expected to be observed³ [see Fig. 7(d)].

Thus, the observation of proton emission from rotational state at spin $I - 8$ and its absence from rotational state at spin $I - 6$, which is possible for the first two cases discussed above, could provide an experimental fingerprint of the transition from proton bound to proton unbound part of rotational band. Note that in all three cases at high spin the rotational states with spins I , $I - 2$, $I - 4$ and $I - 6$ are proton bound since highest in energy occupied proton single-particle state of their configurations is located at negative energy in rotating proton potential [see single-particle states labeled with spins I , $I - 2$, $I - 4$ and $I - 6$ in Fig. 7(b)].

However, this conclusion is complicated by further considerations. Experimental observation of proton emission from the nucleus is possible only when the Q_p energy is located within the Q_p window favorable for the observation of proton emission. The $Q_p(I)$ energies and the $Q_p(I)$ windows are expected to be spin dependent in

rotating nuclei (see Sec. 5.2). This does not represent a problem in rare-earth proton emitters in which the size of the Q_p window is about 0.8–1.7 MeV [79, 82]. However, in the nuclei of interest the Q_p window is significantly smaller⁴ and the transition from the I' to $I' - 2$ state could lead to the situation in which the Q_p value being inside (outside) the Q window at spin I' moves outside (inside) this window at spin $I' - 2$. This is especially the case for light nuclei in which the relative changes in deformation of the states of interest with spin in the parent and daughter nuclei can be very large.

Because of above mentioned extreme sensitivity of proton emission half-lives τ_π to the energies of proton single-particle states, the accurate predictions of the τ_π values are impossible nowadays in any type of theory for the nuclei of interest (even at no rotation). This is because the analysis of the single-particle energies carried out in Refs. [69, 86–89] at and beyond mean field levels clearly indicates that required level of the accuracy in the predictions of the energies of the single-particle states is not achievable in the current generation of the relativistic and non-relativistic DFT models.

However, for light nuclei the situation could be reminiscent to the one expected in neutron rich nuclei in the cases when with the decrease of spin the energy of the highest in energy occupied proton single-particle state in nucleonic configuration exceeds the height of the Coulomb barrier. This is because the height of Coulomb barrier is rather small in such nuclei: for example, it is around 2 MeV in the $N \approx Z$ Ne nuclei (see Fig. 8). Above the Coulomb barrier, proton single-particle states form continuum and the situation is similar to that observed in neutron rich nuclei above continuum threshold. Let us consider the nucleonic configuration the energy of the highest occupied proton single-particle state of which increases with

³This is a reason why rotational structures in proton-unbound ⁵⁹Cu [17] and ¹⁴¹Ho [15] nuclei have been experimentally observed by means of γ -spectroscopy.

⁴The information on the Q_p window is not always provided in the publications. However, it can be evaluated from the comparison of calculated changes in proton emission half-lives with variation of the energy of proton single-particle state in the parent nucleus with present window for the proton emission half-lives ($4.5 \cdot 10^{-7}$ s to few seconds) which can be observed experimentally. For example, the change in proton single-particle energy of around 300 keV in ⁶⁹Br causes a change in the proton decay lifetime of 11 orders of magnitude [79]. This effect is even more pronounced in lighter systems. For example, the variation of the Q_p value between 3 and 50 keV in ⁷B changes the half-lives by 30 orders of magnitude [82]. Note that quoted values are obtained for non-rotating nuclei.

the decrease of rotational frequency Ω [such as for the $\pi 3/2[211](r = -i)$ orbital in the $[0,3]$ configuration of ^{14}Ne (see Fig. 1)]. For some angular frequencies (or spins) this single-particle state is located below the Coulomb barrier but above zero energy threshold. For such spins, the rotational states are discrete and are expected to decay either by proton emission or by γ -decay or by their combination (see discussion above). Let us assume that the lowest in spin rotational state for which such situation holds has the spin I' . With decreasing rotational frequency the energy of the single-particle state of interest will increase above the Coulomb barrier and respective rotational state with spin $I' - 2$ will get some width because of embedment into the continuum. Thus, the abrupt broadening of the $(I') \rightarrow (I' - 2)$ transition at some spin I' with decreasing spin within the rotational band observed in experiment will clearly indicate that such a transition takes place and that the $(I' - 2)$ state becomes a resonance rotational state embedded in continuum. The sequence of rotational states with spin $I' - 2$, $I' - 4$, ... is expected to form the part of rotational band embedded in proton continuum (or resonance band) (see Refs. [13, 90, 91]). Note that with increasing proton number such a transition within the rotational bands of interest becomes less likely because of the raise of Coulomb barrier height (see Fig. 8).

6 Rotation induced extension of the nuclear landscape

An impact of rotation on the properties of very proton rich nuclei similar to that discussed in Sec. 3 has been found for even Z isotopic chains with $4 \leq Z \leq 36$. The detailed results for these and odd Z nuclei will be presented in the follow-up paper [92]. Here, we focus on rotation induced extension of the nuclear landscape presented in Fig. 9. Colored squares or circles in this figure are used for the nuclei which are proton unbound at no rotation, but some configurations of which become proton bound when the nucleus rotates.

The lowest spin ranges (in step of $5\hbar$) at which proton bound configurations appear in the calculations are defined in the following way. In Fig. 9(a), they are shown above the lowest spins I_{unpair} above which the disappearance of static pairing

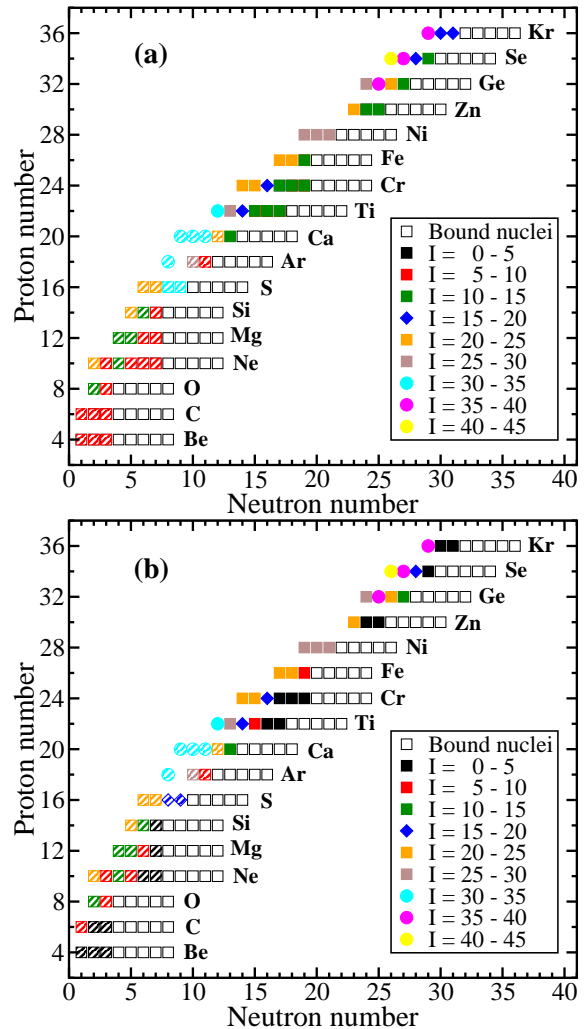


Fig. 9 Rotation induced extension of the nuclear landscape. Open squares show the nuclei which are proton bound at no rotation in the RHB calculations of Ref. [3]; these predictions are compared with experimental data in Sec.VII of Ref. [3]. Colored squares, diamonds and circles show the lowest spin range (in step of $5\hbar$) at which proton bound configurations appear in the calculations (see text for detail). Dashed filling pattern is used to indicate the nuclei in which at least one nucleonic configuration with rotation induced giant proton halo of the types shown in Figs. 4(d) and (e) appear in the calculations.

correlations is expected. The results of the CRHB calculations and the comparison with the ones of the CRMF calculations indicates that static pairing disappears at $I_{unpair} \approx 5\hbar$, $I_{unpair} \approx 10\hbar$ and $I_{unpair} \approx 15\hbar$ in the Ne, Ca and Kr nuclei, respectively (see Refs. [21, 23, 93]). Thus, I_{unpair} is set at $5\hbar$ for the nuclei with $Z \leq 10$ and then gradually increases from $5\hbar$ up to $10\hbar$ for the nuclei

with $12 \leq Z \leq 20$ and from $10\hbar$ up to $15\hbar$ for the nuclei with $22 \leq Z \leq 36$. Note that above these spins we consider not only yrast but also excited configurations which are located not significantly higher than 2 MeV above the yrast line. The configurations located at higher excitation energies are excluded from the analysis since rotational damping may lead to a disappearance of discrete rotational bands [94].

Earlier experience with CRHB and CRMF calculations shows that static pairing correlations could disappear due to combination of blocking and Coriolis anti-pairing effects at spins below I_{unpair} when the configurations are based on particle-hole excitations. Thus, in Fig. 9(b) we also show the lowest spins I_{lowest} ($I_{lowest} < I_{unpair}$) at which such configurations become proton bound in the calculations without pairing. This leads to lowering of the spins as compared with those given in Fig. 9(a) in some nuclei (such as $^{16,17}\text{Ne}$) located close to the proton drip line. The CRHB calculations with pairing are needed to either confirm or reject this lowering of the spins but they go beyond the scope of the present paper. Note that for $I < I_{unpair}$ we consider only the yrast configurations.

Fig. 9 shows that in many nuclei located beyond $I = 0$ proton drip line the transition to proton bound configurations takes place at relatively modest spin values. However, in a given isotopic chain such transition occurs at higher spin values with increasing proton excess. In addition, the calculations suggest that the formation of rotation induced giant proton halos is feasible only in the $Z \leq 20$ nuclei.

7 Conclusions

The detailed investigation of the high-spin properties of proton rich rotating nuclei located at and beyond proton drip line are carried out within the cranked relativistic mean field approach. The main results can be summarized as follows.

- For the first time we show that rotational bands which are proton unbound at zero or low spins can be transformed into proton bound ones by collective rotation of nuclear systems. Strong Coriolis interaction acting on high- N or strongly mixed M orbitals provides a microscopic mechanism for this transformation by

driving the highest in energy occupied single-particle states of nucleonic configurations into negative energy domain. The disappearance of static pairing correlations at high spins of interest is critical for suppression of proton emission from high spin proton bound rotational states. This is because the scattering of particles by pairing interaction from negative energy bound single-particle states to positive energy unbound ones, which would create a proton emission channel from the latter ones, is prohibited in that case. These rotational bands, which undergo the birth of particle bound parts at high spin, are transitional in nature between classical particle bound rotational bands which at present are almost exclusively observed in experiment [34, 39, 40, 94] and very rare examples of rotational bands embedded in particle continuum [90, 91].

- The calculations indicate the presence of rotation induced giant proton halo in the nucleonic configurations which are typically proton bound at high spin. Few of these configurations reveal underlying clustering structures. Their formation is triggered by the occupation of strongly mixed M intruder orbitals. Thus, the physical mechanism of the creation of giant proton halos in rotating nuclei is completely different as compared with non-rotating nuclei in which the formation of proton halo proceeds via the occupation of loosely bound s and p orbitals [70–72].
- Potential experimental signatures of the transition from particle unbound to particle bound part of rotational band have been analyzed in proton and neutron rich nuclei located near and beyond respective spin zero drip lines. The point of the transition from neutron bound to neutron unbound part of rotational band with decreasing spin is uniquely manifest by broadening of the $I' \rightarrow (I' - 2)$ γ -transition. Here, I' ($I' - 2$) is the spin of the lowest in spin neutron bound (highest in spin neutron unbound) rotational state. Such broadening can be measured by means of γ -spectroscopy. In addition, neutron emission is expected from neutron unbound rotational states. The experimental identification of transition point between proton unbound and proton bound parts of rotational band in proton rich nuclei is more complicated. It requires the observation of proton emission from

proton unbound rotational states for which the energies of the highest occupied proton single-particle state are located between zero energy threshold and the height of the Coulomb barrier. The reduction of the lowest experimentally detectable value of τ_π by several orders of magnitude to sub- 10^{-9} s time range is needed for that.

- The birth of proton bound rotational bands leads to a substantial extension of nuclear landscape towards more proton rich nuclei as compared with the one defined in non-rotating nuclei. This is similar to the extension of nuclear landscape towards more proton rich nuclei on transition from ellipsoidal to toroidal shapes in hyperheavy nuclei [10, 12]. In both cases, the change of collective coordinates (deformation in hyperheavy nuclei and combination of deformation and rotational frequency in rotating nuclei) triggers the modification of underlying single-particle structure in such a way that occupied states become proton bound above some values of these coordinates. Note that in a given isotopic chain the transition due to collective rotation to proton bound configurations occurs at higher spin values with increasing proton excess.

This material is based upon work supported by the U.S. Department of Energy, Office of Science, Office of Nuclear Physics under Award No. DE-SC0013037. All authors certify that they have no affiliations with or involvement in any organization or entity with any financial interest or non-financial interest in the subject matter or materials discussed in this manuscript.

References

- [1] T. Baumann, A.M. Amthor, D. Bazin, B.A. Brown, C.M. Folden, A. Gade, T.N. Ginter, M. Hausmann, M. Matos, D.J. Morrissey, M. Portillo, A. Schiller, B.M. Sherrill, A. Stolz, O.B. Tarasov, M. Thoennessen, Discovery of ^{40}Mg and ^{42}Al suggests neutron drip-line slants towards heavier isotopes. *Nature* **449**, 1022 (2007)
- [2] O.B. Tarasov, D.S. Ahn, D. Bazin, N. Fukuda, A. Gade, M. Hausmann, N. Inabe, S. Ishikawa, N. Iwasa, K. Kawata, T. Komatsubara, T. Kubo, K. Kusaka, D.J. Morrissey, M. Ohtake, H. Otsu, M. Portillo, T. Sakakibara, H. Sakurai, H. Sato, B.M. Sherrill, Y. Shimizu, A. Stolz, T. Sumikama, H. Suzuki, H. Takeda, M. Thoennessen, H. Ueno, Y. Yanagisawa, K. Yoshida, Discovery of ^{60}Ca and implications for the stability of ^{70}Ca . *Phys. Rev. Lett.* **121**, 022501 (2018)
- [3] S.E. Agbemava, A.V. Afanasjev, D. Ray, P. Ring, Global performance of covariant energy density functionals: Ground state observables of even-even nuclei and the estimate of theoretical uncertainties. *Phys. Rev. C* **89**, 054320 (2014)
- [4] The science of frib. The science of FRIB; see https://frib.msu.edu/_files/pdfs/frib_scientific_and_technical_merit_lite_0.pdf
- [5] A.V. Afanasjev, S.E. Agbemava, D. Ray, P. Ring, Neutron drip line: Single-particle degrees of freedom and pairing properties as sources of theoretical uncertainties. *Phys. Rev. C* **91**, 014324 (2015)
- [6] J. Erler, N. Birge, M. Kortelainen, W. Nazarewicz, E. Olsen, A.M. Perhac, M. Stoitsov, The limits of the nuclear landscape. *Nature* **486**, 509 (2012)
- [7] E. Olsen, M. Pfützner, N. Birge, M. Brown, W. Nazarewicz, A. Perhac, Landscape of two-proton radioactivity. *Phys. Rev. Lett.* **110**, 222501 (2013)
- [8] L. Neufcourt, Y. Cao, S.A. Giuliani, W. Nazarewicz, E. Olsen, O.B. Tarasov, Quantified limits of the nuclear landscape. *Phys. Rev. C* **101**, 044307 (2020)
- [9] A. Taninah, S.E. Agbemava, A.V. Afanasjev, Covariant density functional theory input for r -process simulations in actinides and superheavy nuclei: The ground state and fission properties. *Phys. Rev. C* **102**, 054330 (2020)
- [10] S.E. Agbemava, A.V. Afanasjev, Hyperheavy spherical and toroidal nuclei: The role of shell structure. *Phys. Rev. C* **103**, 034323 (2021)

- [11] S.E. Agbemava, A.V. Afanasjev, A. Taninah, A. Gyawali, Extension of the nuclear landscape to hyperheavy nuclei. *Phys. Rev. C* **99**, 034316 (2019)
- [12] A.V. Afanasjev, S.E. Agbemava, A. Taninah, Exploring nuclear exotica at the limits. *Acta Phys. Polonica B Proc. Suppl.* **13**, 347 (2020)
- [13] A. Afanasjev, N. Itagaki, D. Ray, Rotational excitations in near neutron-drip line nuclei: The birth and death of particle-bound rotational bands and the extension of nuclear landscape beyond spin zero neutron drip line. *Phys. Lett. B* **794**, 7 (2019)
- [14] F. Kondev, M. Carpenter, R. Janssens, K. Abu Saleem, I. Ahmad, H. Amro, J. Cizewski, M. Danchev, C. Davids, D. Hartley, A. Heinz, T. Khoo, T. Lauritsen, C. Lister, W. Ma, G. Poli, J. Ressler, W. Reviol, L. Riedinger, D. Seweryniak, M. Smith, I. Wiedenhöver, Identification of excited structures in proton unbound nuclei $^{173,175,177}\text{Au}$: shape co-existence and intruder bands. *Phys. Lett. B* **512**, 268 (2001)
- [15] D. Seweryniak, P.J. Woods, J.J. Ressler, C.N. Davids, A. Heinz, A.A. Sonzogni, J. Uusitalo, W.B. Walters, J.A. Caggiano, M.P. Carpenter, J.A. Cizewski, T. Davinson, K.Y. Ding, N. Fotiades, U. Garg, R.V.F. Janssens, T.L. Khoo, F.G. Kondev, T. Lauritsen, C.J. Lister, P. Reiter, J. Shergur, I. Wiedenhöver, Rotational bands in the proton emitter ^{141}Ho . *Phys. Rev. Lett.* **86**, 1458 (2001)
- [16] M. Smith, J. Cizewski, M. Carpenter, F. Kondev, T. Khoo, T. Lauritsen, R. Janssens, K. Abu Saleem, I. Ahmad, H. Amro, M. Danchev, C. Davids, D. Hartley, A. Heinz, C. Lister, W. Ma, G. Poli, J. Ressler, W. Reviol, L. Riedinger, D. Seweryniak, I. Wiedenhöver, Limits of the energy-spin phase space beyond the proton drip line: entry distributions of Pt and Au isobars. *Phys. Lett. B* **551**, 262 (2003)
- [17] D. Rudolph, C. Andreoiu, C. Fahlander, R.J. Charity, M. Devlin, D.G. Sarantites, L.G. Sobotka, D.P. Balamuth, J. Eberth, A. Galindo-Uribarri, P.A. Hausladen, D. Seweryniak, T. Steinhardt, Prompt proton decay scheme of ^{59}Cu . *Phys. Rev. Lett.* **89**, 022501 (2002)
- [18] W. Koepf, P. Ring, A relativistic description of rotating nuclei: the yrast line of ^{20}Ne . *Nucl. Phys. A* **493**, 61 (1989)
- [19] J. König, P. Ring, Identical bands in superdeformed nuclei: A relativistic description. *Phys. Rev. Lett.* **71**, 3079 (1993)
- [20] D. Vretenar, A.V. Afanasjev, G.A. Lalazisis, P. Ring, Relativistic Hartree-Bogoliubov theory: Static and dynamic aspects of exotic nuclear structure. *Phys. Rep.* **409**, 101 (2005)
- [21] A.V. Afanasjev, S. Frauendorf, Description of rotating $N = Z$ nuclei in terms of isovector pairing. *Phys. Rev. C* **71**, 064318 (2005)
- [22] A.V. Afanasjev, Isoscalar and isovector neutron-proton pairing. chapter 11 in the book "50 Years of Nuclear BCS", (World Scientific Publishing Co, Singapore, 2013), p. 138, see also nuclear theory arXiv:1205.2134. (2013)
- [23] D. Ray, A.V. Afanasjev, From superdeformation to extreme deformation and clusterization in the $N \approx Z$ nuclei of the $A \approx 40$ mass region. *Phys. Rev. C* **94**, 014310 (2016)
- [24] P. Ring, P. Schuck, *The Nuclear Many-Body Problem* (Springer-Verlag, Berlin) (1980)
- [25] G.A. Lalazisis, S. Karatzikos, R. Fossion, D.P. Arteaga, A.V. Afanasjev, P. Ring, The effective force NL3 revisited. *Phys. Lett.* **B671**, 36 (2009)
- [26] A.V. Afanasjev, Y. Shi, W. Nazarewicz, Description of ^{158}Er at ultrahigh spin in nuclear density functional theory. *Phys. Rev. C* **86**, 031304(R) (2012)
- [27] A.V. Afanasjev, O. Abdurazakov, Pairing and rotational properties of actinides and superheavy nuclei in covariant density functional theory. *Phys. Rev. C* **88**, 014,320 (2013)

- [28] A.V. Afanasjev, J. König, P. Ring, Superdeformed rotational bands in the $A \sim 140 - 150$ mass region: A cranked relativistic mean field description. *Nucl. Phys. A* **608**, 107 (1996)
- [29] Y. Shi, J. Dobaczewski, S. Frauendorf, W. Nazarewicz, J.C. Pei, F.R. Xu, N. Nikolov, Self-consistent tilted-axis-cranking study of triaxial strongly deformed bands in ^{158}Er at ultrahigh spin. *Phys. Rev. Lett.* **108**, 092501 (2012)
- [30] K. Yoshida, Super- and hyperdeformation in ^{60}Zn , ^{62}Zn , and ^{64}Ge at high spins. *Phys. Rev. C* **105**, 024318 (2022)
- [31] W. Nazarewicz, R. Wyss, A. Johnson, Structure of superdeformed bands in the $A \approx 150$ mass region. *Nucl. Phys. A* **503**, 285 (1989)
- [32] A.V. Afanasjev, H. Abusara, Hyperdeformation in the cranked relativistic mean field theory: The $Z = 40-58$ region of the nuclear chart. *Phys. Rev. C* **78**, 014315 (2008)
- [33] R. Bengtsson, S. Frauendorf, An interpretation of backbending in terms of the crossing of the ground state band with an aligned two-quasiparticle band. *Nucl. Phys. A* **314**, 27 (1979)
- [34] M.J.A. de Voigt, J. Dudek, Z. Szymański, High-spin phenomena in atomic nuclei. *Rev. Mod. Phys.* **55**, 949 (1983)
- [35] Z. Szymański, *Fast nuclear rotation* (Clarendon Press, Oxford, 1983)
- [36] S.G. Nilsson, I. Ragnarsson, *Shapes and shells in nuclear structure*, (Cambridge University Press, 1995)
- [37] J. L. Egido and L. M. Robledo, High spin properties of the Er and Yb isotopes with the Gogny force. *Nucl. Phys. A* **570** 69 (1994)
- [38] B. Gall, P. Bonche, J. Dobaczewski, H. Flocard, P.H. Heenen, Superdeformed rotational bands in the mercury region. a cranked Skyrme-Hartree-Fock-Bogoliubov study. *Zeit. Phys. A* **348**, 183 (1994)
- [39] C. Baktash, B. Haas, W. Nazarewicz, Identical bands in deformed and superdeformed nuclei. *Annu. Rev. Nucl. Part. Sci.* **45**, 485 (1995)
- [40] A.V. Afanasjev, D.B. Fossan, G.J. Lane, I. Ragnarsson, Termination of rotational bands: Disappearance of quantum many-body collectivity. *Phys. Rep.* **322**, 1 (1999)
- [41] S. Frauendorf, Spontaneous symmetry breaking in rotating nuclei. *Rev. Mod. Phys.* **73**, 463 (2001)
- [42] A.V. Afanasjev, P. Ring, J. König, Cranked relativistic hartree-bogoliubov theory: formalism and application to the superdeformed bands in the $A \sim 190$ region. *Nucl. Phys. A* **676**, 196 (2000)
- [43] J. Meng, J. Peng, S.Q. Zhang, P.W. Zhao, Progress on tilted axis cranking covariant density functional theory for nuclear magnetic and antimagnetic rotation. *Front. Phys.* **8**, 55 (2013)
- [44] S. Frauendorf, Beyond the unified model. *Phys. Scr.* **93**, 043,003 (2018)
- [45] A.V. Afanasjev, J. König, P. Ring, Cranked relativistic Hartree-Bogoliubov theory: Superdeformed bands in the $A \sim 190$ region. *Phys. Rev. C* **60**, 051303 (1999)
- [46] A.V. Afanasjev, T.L. Khoo, S. Frauendorf, G.A. Lalazissis, I. Ahmad, Cranked relativistic Hartree-Bogoliubov theory: Probing the gateway to superheavy nuclei. *Phys. Rev. C* **67**, 024309 (2003)
- [47] A.V. Afanasjev, Microscopic description of rotation: From ground states to the extremes of ultra-high spin. *Phys. Scr.* **89**, 054001 (2014)
- [48] Y.K. Wang, Yrast band of ^{109}Ag described by tilted axis cranking covariant density functional theory with a separable pairing force. *Phys. Rev. C* **96**, 054324 (2017)

- [49] B.W. Xiong, Shell-model-like approach based on cranking covariant density functional theory with a separable pairing force. *Phys. Rev. C* **101**, 054305 (2020)
- [50] H. Madokoro, M. Matsuzaki, General relativistic mean field theory for rotating nuclei. *Phys. Rev. C* **56**, R2934 (1997)
- [51] A.V. Afanasjev, I. Ragnarsson, P. Ring, Comparative study of superdeformed and highly deformed bands in the $A \sim 60$ mass region. *Phys. Rev. C* **59**, 3166 (1999)
- [52] A.V. Afanasjev, G. Lalazissis, P. Ring, Relativistic mean field theory in rotating frame: Single-particle properties at superdeformation. *Nucl. Phys. A* **634**, 395 (1998)
- [53] A.V. Afanasjev, S. Frauendorf, Superdeformation and hyperdeformation in the ^{108}Cd nucleus. *Phys. Rev. C* **72**, 031301 (2005)
- [54] M. Matev, A.V. Afanasjev, J. Dobaczewski, G.A. Lalazissis, W. Nazarewicz, Additivity of effective quadrupole moments and angular momentum alignments in $A \sim 130$ nuclei. *Phys. Rev. C* **76**, 034304 (2007)
- [55] I. Ragnarsson, Orbital and spin assignment of SD bands in the Dy/Gd region of identical bands. *Nucl. Phys. A* **557**, c167 (1993)
- [56] W. Satuła, J. Dobaczewski, J. Dudek, W. Nazarewicz, Additivity of quadrupole moments in superdeformed bands: Single-particle motion at extreme conditions. *Phys. Rev. Lett.* **77**, 5182 (1996)
- [57] A.V. Afanasjev, Model of independent particle motion. in "Handbook on Nuclear Physics", edited by I. Tanihata, H. Toki, and T. Kajino (Springer, Singapore, 2022). This publication is available in electronic form at https://doi.org/10.1007/978-981-15-8818-1_10-1
- [58] E. Caurier, F. Nowacki, A. Poves, J. Retamosa, Shell model study of the neutron rich isotopes from oxygen to silicon. *Phys. Rev. C* **58**, 2033 (1998)
- [59] T. Otsuka, T. Suzuki, J.D. Holt, A. Schwenk, Y. Akaishi, Three-body forces and the limit of oxygen isotopes. *Phys. Rev. Lett.* **105**, 032501 (2010)
- [60] P. Maris, M.A. Caprio, J.P. Vary, Emergence of rotational bands in ab initio no-core configuration interaction calculations of the be isotopes. *Phys. Rev. C* **91**, 014310 (2015)
- [61] D. Rudolph, C. Baktash, M.J. Brinkman, E. Caurier, D.J. Dean, M. Devlin, J. Dobaczewski, P.H. Heenen, H.Q. Jin, D.R. LaFosse, W. Nazarewicz, F. Nowacki, A. Poves, L.L. Riedinger, D.G. Sarantites, W. Satuła, C.H. Yu, Rotational bands in the doubly magic nucleus ^{56}Ni . *Phys. Rev. Lett.* **82**, 3763 (1999)
- [62] Y. Tsunoda, T. Otsuka, N. Shimizu, M. Honma, Y. Utsuno, Novel shape evolution in exotic Ni isotopes and configuration-dependent shell structure. *Phys. Rev. C* **89**, 031301 (2014)
- [63] K. Hara, Y. Sun, Projected shell model and high-spin spectroscopy. *Int. J. Mod. Phys. E* **4**, 637 (1995)
- [64] J.A. Sheikh, G.H. Bhat, R. Palit, Z. Naik, Y. Sun, Multi-quasiparticle γ -band structure in neutron-deficient ce and nd isotopes. *Nucl Phys. A* **824**, 58 (2009)
- [65] T. Goigoux, P. Ascher, B. Blank, M. Gerbaux, J. Giovinazzo, S. Grévy, T. Kurtukian Nieto, C. Magron, P. Doornenbal, G.G. Kiss, S. Nishimura, P.A. Söderström, V.H. Phong, J. Wu, D.S. Ahn, N. Fukuda, N. Inabe, T. Kubo, S. Kubono, H. Sakurai, Y. Shimizu, T. Sumikama, H. Suzuki, H. Takeda, J. Agramunt, A. Algora, V. Guadilla, A. Montaner-Piza, A.I. Morales, S.E.A. Orrigo, B. Rubio, Y. Fujita, M. Tanaka, W. Gelletly, P. Aguilera, F. Molina, F. Diel, D. Lubos, G. de Angelis, D. Napoli, C. Borcea, A. Boso, R.B. Cakirli, E. Ganioglu, J. Chiba, D. Nishimura, H. Oikawa, Y. Takei, S. Yagi, K. Wimmer, G. de France, S. Go, B.A. Brown, Two-proton radioactivity of ^{67}Kr . *Phys. Rev. Lett.* **117**, 162501 (2016)

- [66] S.M. Wang, W. Nazarewicz, Puzzling two-proton decay of ^{67}Kr . *Phys. Rev. Lett.* **120**, 212502 (2018)
- [67] A. Taninah, S.E. Agbemava, A.V. Afanasjev, P. Ring, Parametric correlations in energy density functionals. *Phys. Lett. B* **800**, 135065 (2020)
- [68] P.G. Reinhard, M. Rufa, J. Maruhn, W. Greiner, J. Friedrich, Nuclear ground state properties in a relativistic meson field model. *Z. Phys. A* **323**, 13 (1986)
- [69] A.V. Afanasjev, S. Shawaqfeh, Deformed one-quasiparticle states in covariant density functional theory. *Phys. Lett. B* **706**, 177 (2011)
- [70] B. Brown, P. Hansen, Proton halos in the $1s0d$ shell. *Phys. Lett. B* **381**, 391 (1996)
- [71] X.Z. Cai, H.Y. Zhang, W.Q. Shen, Z.Z. Ren, J. Feng, D.Q. Fang, Z.Y. Zhu, W.Z. Jiang, Y.G. Ma, C. Zhong, W.L. Zhan, Z.Y. Guo, G.Q. Xiao, J.S. Wang, Y.T. Zhu, J.C. Wang, J.X. Li, M. Wang, J.F. Wang, Z.J. Ning, Q.J. Wang, Z.Q. Chen, Existence of a proton halo in ^{23}Al and its significance. *Phys. Rev. C* **65**, 024610 (2002)
- [72] A.S. Jensen, K. Riisager, D.V. Fedorov, E. Garrido, Structure and reactions of quantum halos. *Rev. Mod. Phys.* **76**, 215 (2004)
- [73] A.V. Afanasjev, H. Abusara, From cluster structures to nuclear molecules: The role of nodal structure of the single-particle wave functions. *Phys. Rev. C* **97**, 024329 (2018)
- [74] R. Bengtsson, S. Frauendorf, Quasiparticle spectra near the yrast line. *Nucl. Phys. A* **327**, 139 (1979)
- [75] A. Valor, J.L. Egido, L.M. Robledo, Approximate particle number projection with density dependent forces: Superdeformed bands in the $A = 150$ and $A = 190$ regions. *Nucl. Phys. A* **665**, 46 (2000)
- [76] Z.H. Zhang, M. Huang, A.V. Afanasjev, Rotational excitations in rare-earth nuclei: A comparative study within three cranking models with different mean fields and treatments of pairing correlations. *Phys. Rev. C* **101**, 054303 (2020)
- [77] A.V. Afanasjev, P. Ring, Superdeformations in relativistic and non-relativistic mean field theories. *Phys. Scripta* **T88**, 10 (2000)
- [78] E. Caurier, J.L. Egido, G. Martínez-Pinedo, A. Poves, J. Retamosa, L.M. Robledo, A.P. Zuker, Intrinsic vs laboratory frame description of the deformed nucleus ^{48}Cr . *Phys. Rev. Lett.* **75**, 2466 (1995)
- [79] P.J. Woods, C.N. Davids, Nuclei beyond the proton drip-line. *Ann. Rev. Nucl. Part. Sc.* **47**, 541 (1997)
- [80] K. Auranen, A.D. Briscoe, L.S. Ferreira, T. Grahn, P.T. Greenlees, A. Herzán, A. Illana, D.T. Joss, H. Joukainen, R. Julin, H. Jutila, M. Leino, J. Louko, M. Luoma, E. Maglione, J. Ojala, R.D. Page, J. Pakarinen, P. Rahkila, J. Romero, P. Ruotsalainen, M. Sandzelius, J. Sarén, A. Tolosa-Delgado, J. Uusitalo, G. Zimba, Nanosecond-scale proton emission from strongly oblate-deformed ^{149}Lu . *Phys. Rev. Lett.* **128**, 112501 (2022)
- [81] D.S. Delion, R.J. Liotta, R. Wyss, Theories of proton emission. *Phys. Rep.* **424**, 113 (2006)
- [82] S. Åberg, P.B. Semmes, W. Nazarewicz, Spherical proton emitters. *Phys. Rev. C* **56**, 1762 (1997)
- [83] P. Arumugam, L.S. Ferreira, E. Maglione, Fine structure in proton radioactivity: An accurate tool to ascertain the breaking of axial symmetry in ^{145}Tm . *Phys. Rev. C* **78**, 041305 (2008)
- [84] A. Volya, C. Davids, Nuclear pairing and Coriolis effects in proton emitters. *Eur. Phys. J.* **A25**, 161 (2005)
- [85] P. Arumugam, L.S. Ferreira, E. Maglione, Proton emission, gamma deformation, and the spin of the isomeric state of ^{141}Ho . *Phys. Lett. B* **680**, 443 (2009)

- [86] E.V. Litvinova, A.V. Afanasjev, Dynamics of nuclear single-particle structure in covariant theory of particle-vibration coupling: From light to superheavy nuclei. *Phys. Rev. C* **84**, 014305 (2011)
- [87] A.V. Afanasjev, E. Litvinova, Impact of collective vibrations on quasiparticle states of open-shell odd-mass nuclei and possible interference with the tensor force. *Phys. Rev. C* **92**, 044317 (2015)
- [88] D. Tarpanov, J. Dobaczewski, J. Toivanen, B.G. Carlsson, Spectroscopic properties of nuclear skyrme energy density functionals. *Phys. Rev. Lett.* **113**, 252501 (2014)
- [89] J. Dobaczewski, A.V. Afanasjev, M. Bender, L.M. Robledo, Y. Shi, Properties of nuclei in the nobelium region studied within the covariant, Skyrme, and Gogny energy density functionals. *Nucl. Phys. A* **944**, 388 (2015)
- [90] E. Garrido, A.S. Jensen, D.V. Fedorov, Rotational bands in the continuum illustrated by ⁸Be results. *Phys. Rev. C* **88**, 024001 (2013)
- [91] K. Fosse, W. Nazarewicz, Y. Jaganathen, N. Michel, M. Płoszajczak, Nuclear rotation in the continuum. *Phys. Rev. C* **93**, 011305 (2016)
- [92] S. Teeti, A. Taninah, A. Afanasjev, in preparation
- [93] C. Andreoiu, C.E. Svensson, A.V. Afanasjev, R.A.E. Austin, M.P. Carpenter, D. Dashdorj, P. Finlay, S.J. Freeman, P.E. Garrett, J. Greene, G.F. Grinyer, A. Gørgen, B. Hyland, D. Jenkins, F. Johnston-Theasby, P. Joshi, A.O. Machiavelli, F. Moore, G. Mukherjee, A.A. Phillips, W. Reviol, D.G. Sarantites, M.A. Schumaker, D. Seweryniak, M.B. Smith, J.J. Valiente-Dobón, R. Wadsworth, High-spin lifetime measurements in the $N = Z$ nucleus ⁷²Kr. *Phys. Rev. C* **75**, 041301 (2007)
- [94] T. Døssing, B. Herskind, S. Leoni, A. Bracco, R. Broglia, M. Matsuo, E. Vigezzi, Fluctuation analysis of rotational spectra. *Phys. Rep.* **268**, 1 (1996)